agronomy

MDPI

Article

The More Fractal the Architecture the More Intensive the Color of Flower: A Superpixel-Wise Analysis towards High-Throughput Phenotyping

Jardel da Silva Souza [1,*], Laura Monteiro Pedrosa [2], Bruno Rafael de Almeida Moreira [1], Elizanilda Ramalho do Rêgo [2] and Sandra Helena Unêda-Trevisoli [1]

[1] School of Agricultural and Veterinary Sciences, São Paulo State University (Unesp), Jaboticabal 14884-900, SP, Brazil; b.moreira@unesp.br (B.R.d.A.M.); shu.trevisoli@unesp.br (S.H.U.-T.)
[2] Center for Agricultural Sciences, Federal University of Paraíba (UFPB), Areia 58397-000, PB, Brazil; pedrosamlaura@gmail.com (L.M.P.); elizanilda@cca.ufpb.br (E.R.d.R.)
* Correspondence: jardel.souza@unesp.br

Abstract: A breeder can select a visually appealing phenotype, whether for ornamentation or landscaping. However, the organic vision is not accurate and objective, making it challenging to bring a reliable phenotyping intervention into implementation. Therefore, the objective of this study was to develop an innovative solution to predict the intensity of the flower's color upon the external shape of the crop. We merged the single linear iterative clustering (SLIC) algorithm and box-counting method (BCM) into a framework to extract useful imagery data for biophysical modeling. Then, we validated our approach by fitting Gompertz function to data on intensity of flower's color and fractal dimension (S^D) of the architecture of white-flower, yellow-flower, and red-flower varieties of *Portulaca umbraticola*. The SLIC algorithm segmented the images into uniform superpixels, enabling the BCM to precisely capture the S^D of the architecture. The S^D ranged from 1.938315 to 1.941630, which corresponded to pixel-wise intensities of 220.85 and 47.15. Thus, the more compact the architecture the more intensive the color of the flower. The sigmoid Gompertz function predicted such a relationship at $r_{adj}{}^2 > 0.80$. This study can provide further knowledge to progress the field's prominence in developing breakthrough strategies toward improving the control of visual quality and breeding of ornamentals.

Keywords: box-counting method; fractal geometry theory; imagery processing; *Portulaca umbraticola*; superpixel segmentation

Citation: Souza, J.d.S.; Pedrosa, L.M.; Moreira, B.R.d.A.; Rêgo, E.R.d.; Unêda-Trevisoli, S.H. The More Fractal the Architecture the More Intensive the Color of Flower: A Superpixel-Wise Analysis towards High-Throughput Phenotyping. *Agronomy* **2022**, *12*, 1342. https://doi.org/10.3390/agronomy12061342

Academic Editor: Mario Cunha

Received: 15 April 2022
Accepted: 27 May 2022
Published: 31 May 2022

1. Introduction

Experts prospect that both thinking and making in agriculture will not be easy in the near future [1–4]. Climate change (e.g., heat waves, droughts, and flooding), economic crises, and civil conflicts (e.g., wars) will make it harder for farmers to produce goods and services in a sustainable way [5–7]. Therefore, stakeholders (e.g., the scientific community, policymakers, and civil society) in the global agriculture system must be aware of the commitment, cooperation, and coordination they need to elaborate to effectively strengthen the production and distribution of sufficient quantities of affordable goods and services to all [8,9]. They need to take a proactive and stringent stance to promote and perpetuate transformative agriculture via strategic, catalytic, and resilience-building interventions [10,11]. For instance, a breakthrough solution to farming in a challenging world would be genetic breeding, whether for developing future-ready genotypes or highly valuable special crops such as ornamentals [12–14].

The action of genetically breeding a plant can enable stakeholders to either maximize yield and quality or minimize losses and costs. thereby, leveling up the agronomic return

on infrastructural investments. However, it can be costly, time-consuming, and labor-intensive [12]. A genetic breeding program often demands a professional staff to operate or proceed in a successful way [14]. An analyst can visually inspect an outstanding plant and select it phenotypically. However, the organic vision is not precise and objective, making it challenging to bring a reliable phenotyping intervention into implementation [12,14]. Furthermore, the staff may need to invasively intervene in the breeding facility by touching the object [12,14]. Therefore, our timely study will develop and demonstrate the potential of a cutting-edge imagery protocol to accurately and realistically model the intensity of a flower's color upon the architectural complexity of an ornamental commodity, namely *Portulaca umbraticola*.

P. umbraticola is a member of Portulacaceae [15]. It is an herb and often produces showy (vibrant) flowers, which are a wealth of natural beauty and visually appealing to attract stakeholders (e.g., commodity sellers and buyers) at markets of ornamentation and landscaping [13]. Research and biotechnological development into large-scale high-throughput genotyping/phenotyping for mainstream ornamental crops are mature [13,16]. In contrast, the scientific community is not likely to place an adequate emphasis on *P. umbraticola*. Insufficient literature on conventional and high-throughput phenotyping for *P. umbraticola* can make it challenging to ground our study on a consistent base of research into actionable state-of-the-art techniques of particular relevance to such a crop. However, by reviewing full-text articles on high-throughput phenotyping, we can identify the processing of images as an enabler for computationally measuring the external shape of *Yucca* spp. [17], detecting the physiological maturation of *Passiflora* spp. upon spectral imagery data [18], and predicting the quality of *Actinidia* spp. upon high-resolution hyperspectral data [19]. The authors underline the importance of the processing of the digital image to provide useful data in order to bring accurate and reliable biophysical models into implementation. They also stress the relevance of elaborating a sequence of instructions capable of working on the space of analysis, without bias and computational unfeasibility. Furthermore, they point out the importance of caring about the choice of suitable descriptors to prevent algorithms from underfitting or overfitting imagery data.

For instance, flowers are diverse both genotypically and phenotypically. They display a wide range of colors, shapes, and sizes. Particularly for ornamental commodities, such reproductive structures are crucial to determine the price and acceptance of the product in the market [20]. The color of the flower and degree of architectural compactness can interact with another flower and control the visual quality of ornamentals through the transportation and allocation of photo-assimilates [21–24]. However, these morphophysiological descriptors are subjective to the organic vision [17]. Thus, employing them as botanical descriptors in the conventional selection of an outstanding phenotype, whether for ornamentation or landscaping, can bias the breeding intervention and so the analyst will not be likely to succeed in positioning a trustworthy solution in the real world [25]. Even though the processing of the image is a powerful movement towards transforming the representation of a fractal pattern into a higher level of abstraction, an unsuitable descriptor, such as the architecture in the volumetric modeling for apple [26], prediction of biomass for rice [27] and microstructural characterization of leaves for *Anacardium occidentale* [28], can make it challenging for cutting-edge algorithms to effectively map a set of inputs to an output.

Therefore, considering the research and development of high-throughput phenotyping, the primary objective of our explanatory study was to develop an imagery protocol to predict the pixel-wise intensity of flower's color upon the fractality of the architecture of *P. umbraticola*. A secondary objective was to analyze whether the color of the flower can impact the modeling and the effectiveness of superpixel segmentation in isolating potential botanical confounders.

2. Materials and Methods

2.1. Acquisition of Imagery Data

We set up our "photography studio" in a place with the greatest possible source of nature, since this is key to acquiring useful imagery data [17]. Once we have decided which had the best natural light to take pictures, we set up the best backdrop for our photographic style and theme. The backdrop consisted of a dark stretchy fabric, which does not reflect light when shooting and can add more excitement to images. Once we had wondered what shooting device we might need for our study, we employed a professional camera (Canon EOS Rebel T6i), which has technical specifications of 3:2 horizontal/vertical ratio, 6000 × 4000 pixels, and 10.6 diagonal inches at 8.78" width × 5.86" length and can provide up to 600 dpi resolution; however, once we had set the size of the digital representation of an image to 8.27" width × 11.69" length (A4 format), we acquired 24-bit-color photos at the maximum pixel density of 484 dpi. An RBG display system (8 bits for each red, blue and green subpixel) with at least 300 dpi can provide useful imagery data for processing and modeling [17]. We set up the camera onto a tripod, positioned the samples of *P. umbraticola* in the work-up zone, then photographed them from varying angles to capture the qualities of the subject of study at eye level, overhead, and from lower positions. We uploaded the photos to a personal computer, then saved them as a PNG, which is a raster-graphic format file supporting lossless data compression. To acquire imagery data, we organized the samples by the color of the flower into groups, namely white, yellow, and red. Every group consisted of ten samples to control for any systematic error. We grew the varieties of *P. umbraticola* in pots in a glasshouse, managing them with the best agronomic practices, including irrigation, fertilization, and weeding. Thereby, we selected the most visually appealing individuals to prepare samples for taking photos without any interference from environmental degradation or noise.

2.2. Processing of Imagery Data

The processing of 24-bit-color images consisted of the following major steps: labeling (A), equalization (B), quantization (C), segmentation (D), and binarization (E). The objective of labeling was to assign the digital representation of an image to a variety or group by the color of the flower. The role of equalization was to improve the contrast of an image by effectively spreading out the most frequent values or intensity or stretching out the range of luminance in a histogram [29]. The objective of quantization was to compress distinctive discrete symbols into a single quantum value, providing sufficient information in a new representation visually similar to the original [30] for the measuring of the intensity values of pixels within superpixels; we programmatically performed the partitioning of images through the SLIC algorithm, which can group pixels by color similarity or topological proximity merely as a result of processing low-intensity regions in the space of analysis without any computational unfeasibility [31]. The binarization consisted of computationally transforming the entire 24-bit-color graphics into a collection of pixels into black and white corresponding to the subject of study and the background [32], thereby separating the region of interest for further processing. We performed the binarization to determine the fractal dimension of the external shape of *P. umbraticola* through the box-counting method (BCM) (Figure 1).

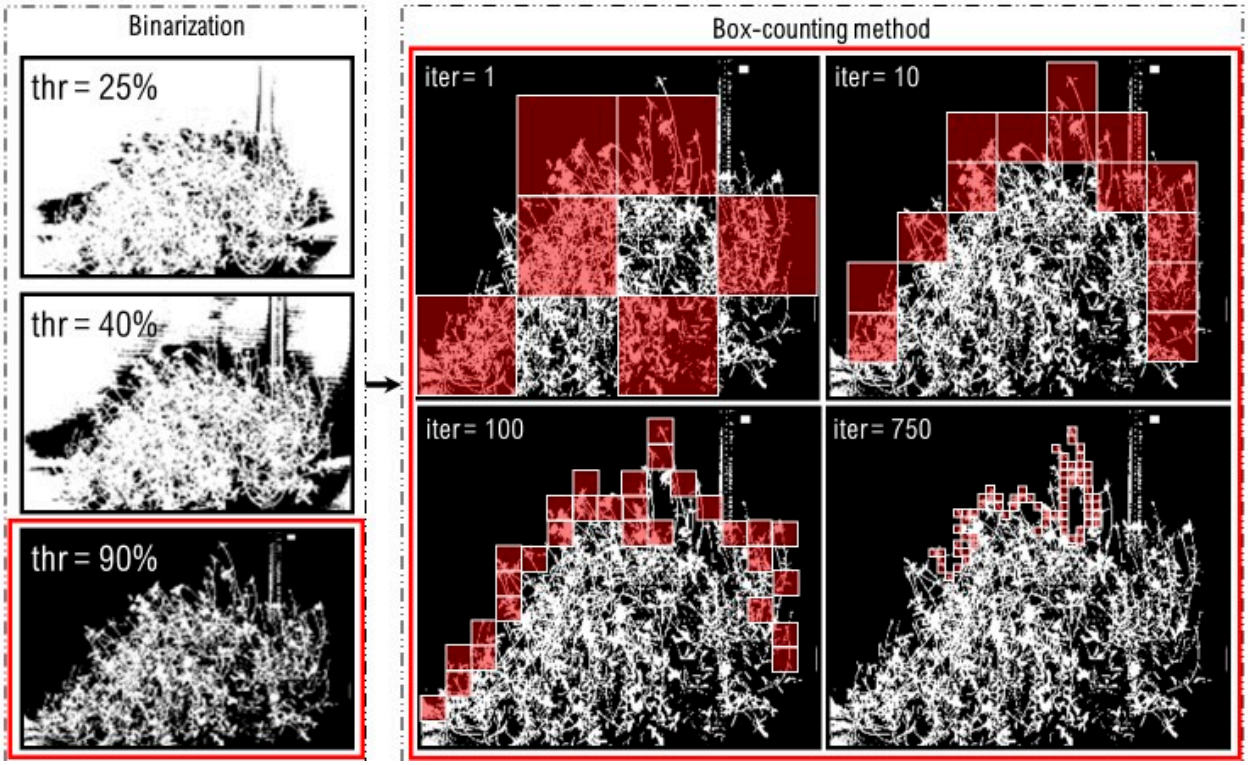

Figure 1. Example of binarizing a 24-bit-color image into a collection of pixels in black and white to determine the fractal dimension of the architecture of *P. umbraticola*. The set of thresholds (thr) for the binarization is defined automatically between 5–95% of the highest intensity values of pixels, with an interval of 5% for standardization. The best output of binarization becomes the input for the determination of the fractal dimension of the external shape of *P. umbraticola* through BCM. The box-counting algorithm processes the image iteratively (iter) until it completely covers the pattern at the border or region of interest to precisely describe the external shape, as opposed to global measures to describe the entire subject of analysis.

The standard operating mode of BCM is to scan the image in a non-overlapping and lattice pattern. However, the algorithm is flexible and can be readjusted to lay boxes over a digital representation concentrically focused on a region of interest, such as a visually irregular external shape of *P. umbraticola*. Thereby, we binarized the image at varying thresholds between 5–95% of the highest intensity values of pixels with an interval of 5% for standardization; then, we selected the best binary contours to capture the fractal dimension at local regions to precisely assess the external shape of the subject of study, as opposed to global measures to describe the entire pattern. As original photos were two-dimensional color graphics, values of fractal dimension (S^D) should range from 1 to 2. The closer to 1 the value of S^D the smoother or less fractal the contour, and thus the *P. umbraticola* becomes architecturally less complex or more regular in external shape. In contrast, the closer to 2 the value of S^D the rougher or more fractal the contour, as the number of boxes of finer grids necessary for assessing the local variation increases, and thus the *P. umbraticola* becomes architecturally more complex or irregular in external shape. The BCM determines the S^D of the pattern iteratively by covering it and then quantifying the number of boxes touching it at the border or region of interest in the topological space of a 2D image. Graphically, the S^D is the slope of the curve when we plot the number of boxes (N_s) on the y-axis against the size of the box (s) on the x-axis. By shrinking the size of boxes, we can more accurately capture the S^D of the pattern at decreasing multiple

scales [33]. We can describe the S^D by an equation (Equation (1)) involving the natural logarithm of both N_s and s.

$$S^D = \lim_{n\to\infty}\left[\frac{ln(N_s)}{ln(s)}\right] \quad (1)$$

The intensity value of each pixel in the image is a single value for a grey-level image or a set of values for a color image [34], such as a 24-bit-color or binary digital representation for *P. umbraticola*. Thereby, we decided to include the linear filter method in the programmatic measurement of intensity values of pixels within superpixels, with features similar to those of the original photos. To the best of our knowledge, the linear filter is the simplest method of averaging an image by itself, by which the intensity values of pixels can be determined merely as a result of processing their neighboring pixels within a specific region [35]. We can describe the linear filter by an equation (Equation (2)) involving the intensity value of pixel, size, and weighting of the filter. By analyzing the equation, the default behavior of the linear filter method is to measure the total intensity of the target region in the image by summing all pixel-wise intensities and then dividing all pixels by the maximum possible intensity value. The user can measure all pixels in the entire image, or restrict the processing within specific regions, as we carried out within superpixels. If the image is segmented, only superpixels will be measured computationally from an area of interest centered on the pixel, improving the process [34,35].

$$f'(x,y) = \sum_{i=-M}^{+M}\sum_{j=-M}^{+M} w_{i,j} f(x+i, y+j) \Big/ \sum_{i=-M}^{+M}\sum_{j=-M}^{+M} w_{i,j} \quad (2)$$

where $f(x, y)$ is the intensity value of pixel (x, y), while M is the size of the filter and w represents the weighting of the filter.

2.3. Data Analytics

We ran PCA as a multi-dimensional statistical approach to establish a functional relationship between the pixel-wise intensity of the color of the botanical descriptors, namely corolla, sepal, petal, and filament, and the fractal dimension of the architecture. Another objective of applying PCA was to capture graphically the effect of potentially confounding features of anatomy in the quality of data without adequate processing, and how this could bias the outcome of multivariate data analytics. Furthermore, we fitted the sigmoid Gompertz function (Equation (2)) to imagery data with and without over-segmentation to more precisely and realistically model the intensity-fractality nexus and validate the importance of the SLIC algorithm to our cutting-edge approach; the metric to analyze the adequacy was the adjusted coefficient of determination (r_{adj}^2). We performed all analyzes in the environment of the R-project for statistical computing and graphics [36].

$$f_x = \alpha e^{-\beta e^{-kx}} \quad (3)$$

where f_x is the dependent variable, x is the independent variable, α is the asymptote, β is the inflection point, k is the exponential decay of specific-growth rate, and e is the Euler constant [37].

3. Results

3.1. The Anatomy of Flower and Architecture of P. umbraticola

The portable shooting device allowed for capturing high-resolution photographs from individuals of *P. umbraticola* (Figure 2); hence, it produced useful imagery data for processing and biophysical modeling.

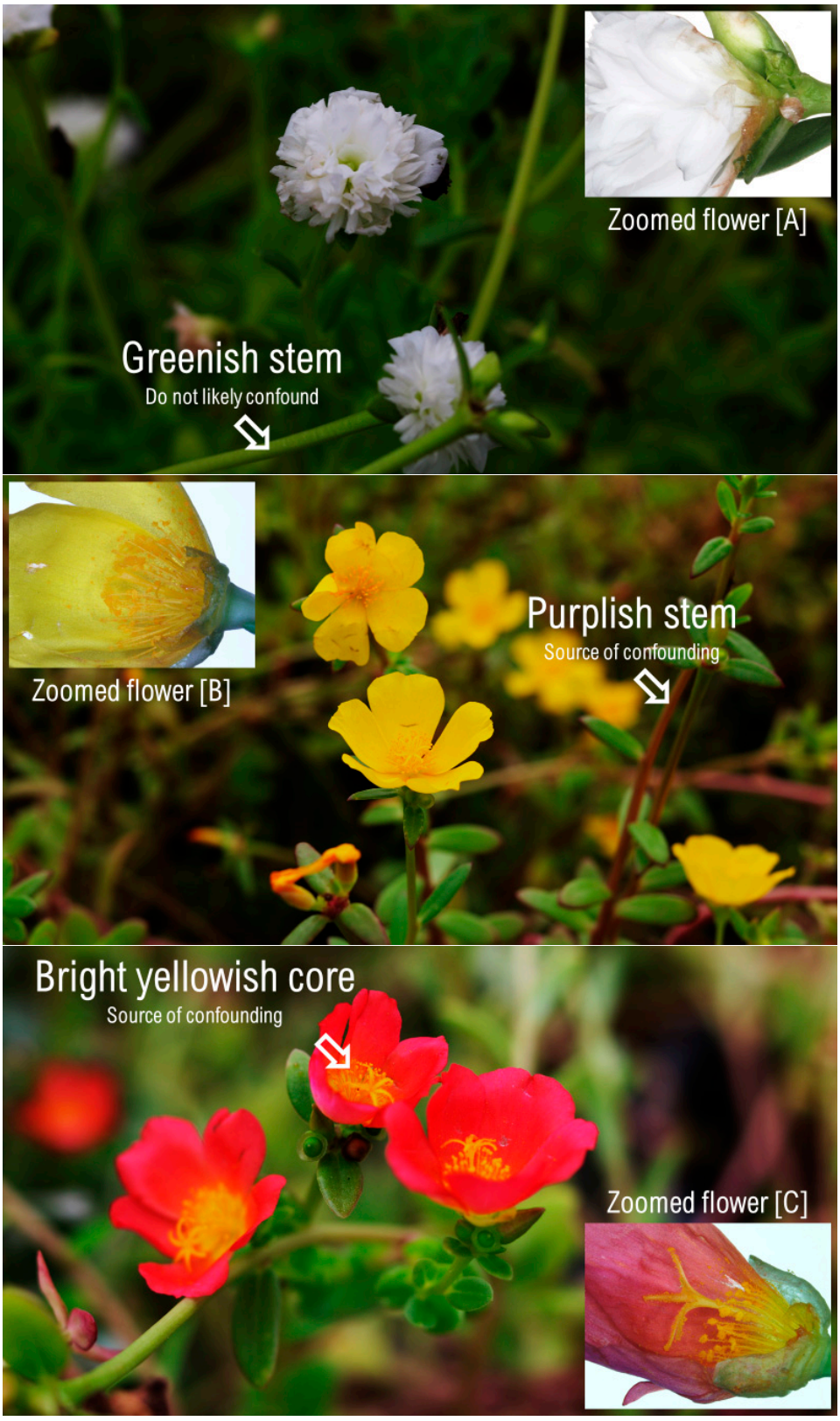

Figure 2. High-resolution digital representation of the anatomy of flowers and architecture of white-flower (**A**), yellow-flower (**B**), and red-flower (**C**) varieties of *P. umbraticola*. Arrows in the diagram visually assign the sources of confounding (non-random variability or unrealistic structural output-to-input dependency) to the processing of images.

By analyzing the high-resolution digital photos, flowers were readily recognizable from the top of the plant, irrespective of the variety. By contrast, sepals, petals, filaments, and anthers as the prominent constitutive features of the flower were not easily identifiable from the representation of an image, although they were accessible in the vision of the observer. Furthermore, leaves and stems (purplish in red-flower and yellow-flower varieties and greenish in the white-flower variety) did influence the vegetative portion of samples, making it possible to characterize them architecturally by processing imagery data on BCM. Values of S^D ranged from 1.938315 to 1.941630, supporting the irregular character of the architecture.

3.2. Mapping the Flower's Color to Canopy's Architecture over a Pixel-Wise Intensity-Fractality Nexus

The PCA reduced the dimensionality of original image data while exporting only useful statistics into the orthogonal subsets, namely PC_I and PC_{II}. Such latent hits together explained 83.40% (Table S1, Supplementary Materials) of the total variability in the intensity–fractality nexus, thereby, supporting a reliable multivariate analysis.

The primary component had positive linear relationships with corolla (r = 0.95; *p*-value < 0.05), petal (r = 0.90; *p*-value < 0.05), filament (r = 0.80; *p*-value < 0.05) and anther (r = 0.80; *p*-value < 0.05). In contrast, it had a negative correlation with the S^D (r = 0.70; *p*-value < 0.05), making it attributable to the architecture's compactness (Table S1, Supplementary Materials). Therefore, by analyzing the structure of PC_I, the larger the S^D the more irregular the plant and thus it does not relate to high-intensity pixels corresponding to parts of the flower. The antagonistic relationship between S^D and both corolla and petal in the second dimension of the factorial map (Figures 3–5) further supported the role of architecture in determining the intensity of the flower's color. The PC_{II} had positive correlations with corolla (r = 0.85; *p*-value < 0.05) and petal (r = 0.75; *p*-value < 0.05). In contrast, it had negative linear relationships with the S^D (r = 0.75; *p*-value < 0.05), anther (r = 0.65; *p*-value < 0.05) and filament (r = 0.70; *p*-value < 0.05) (Table S1, Supplementary Materials), thereby, making it attributable to intensity of color. Corolla, petal, and S^D proved to be the most reliable botanical and computational descriptors for flower's color and canopy's architecture. Such eigenvectors respectively represented 25.1%, 14.5%, and 12% of the total variance in PC_I, and 20.5%, 11.2%, and 9.3% of the total variance in PC_{II} (Table S1, Supplementary Materials).

Another significant computational descriptor for the modeling refers to pixel intensity. By analyzing the factorial map for white-flower samples (Figure 3), the larger the proportion of high-intensity pixels in the upper right quadrant, the more compact the architecture and the more intensive the flower's color. In contrast, low-intensity pixels describe the proportion of either background or vegetative organs in the digital representation of an image. For instance, photogrammetric reconstruction of white-flower samples in the right lower sublevel map of the "eye-catching" panel (Figure 3D) consisted of a larger proportion of low-intensity pixels, because they produced less showy flowers and were structured via the most irregular external shape. In contrast, the photogrammetric reconstruction of white-flower samples in the left upper sublevel map (Figure 3A) consisted of a lower proportion of low-intensity pixels, since they produced the largest quantity of showy flowers and structured via the most uniform architecture.

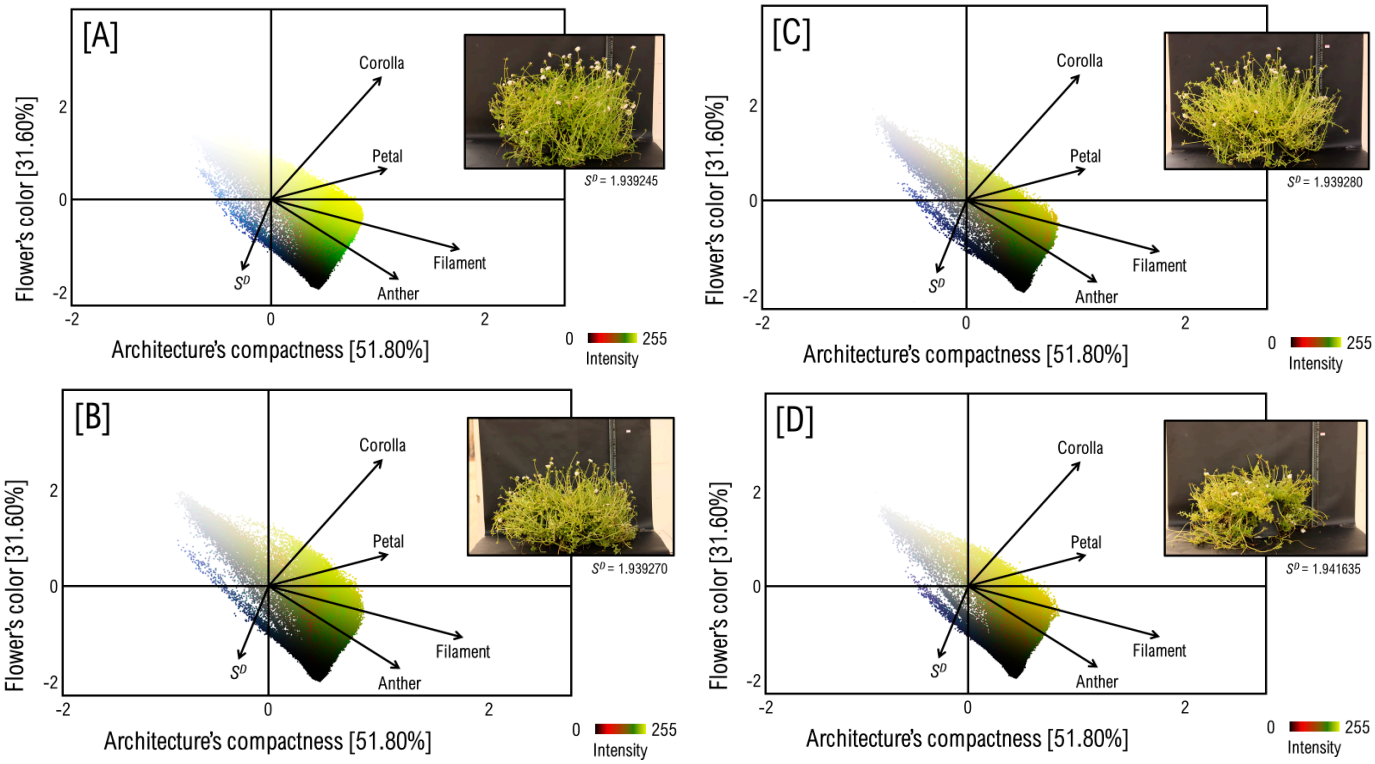

Figure 3. Mapping the botanical and computational features of flower and the architecture of white-flower samples of *P. umbraticola*. The sequence of alphanumerical symbols, from (**A**–**D**), relates to the increasing fractality of the pattern in the representation of the digital image.

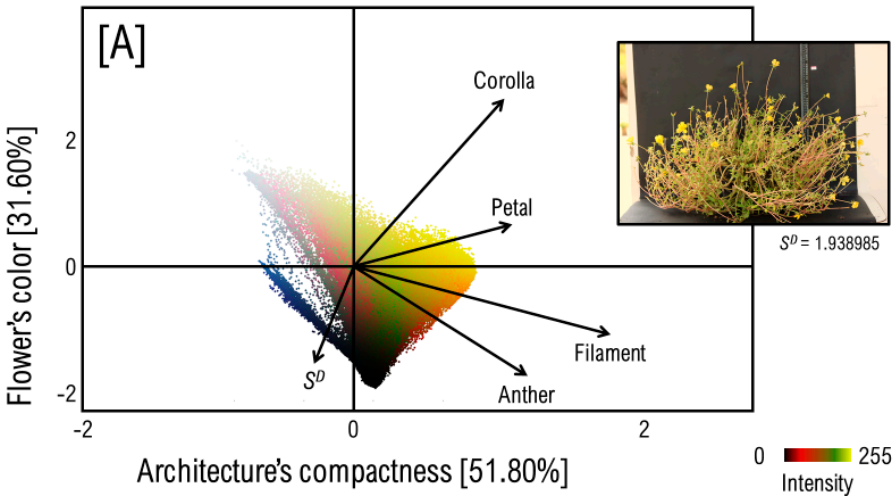

Figure 4. *Cont.*

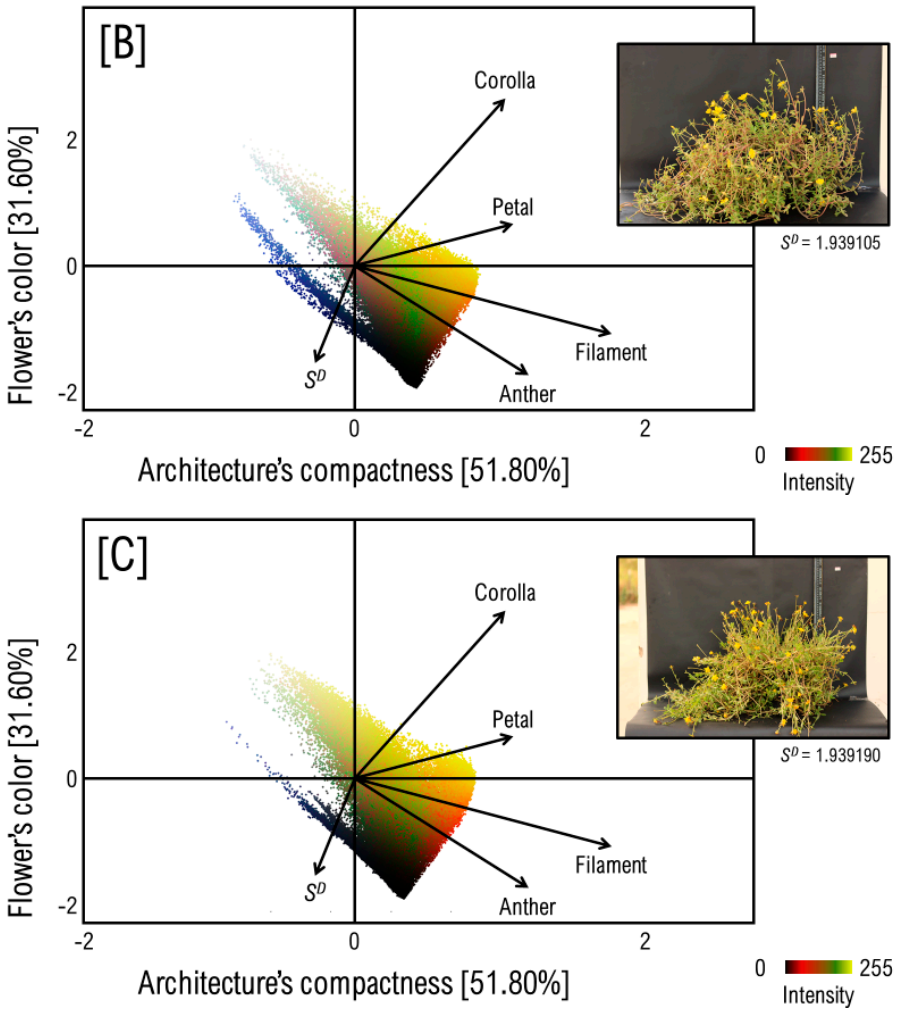

Figure 4. Mapping the botanical and computational features of flower and the architecture of yellow-flower samples of *P. umbraticola*. The sequence of alphanumerical symbols, from (**A**–**C**), relates to the increasing fractality of the pattern in the representation of the digital image.

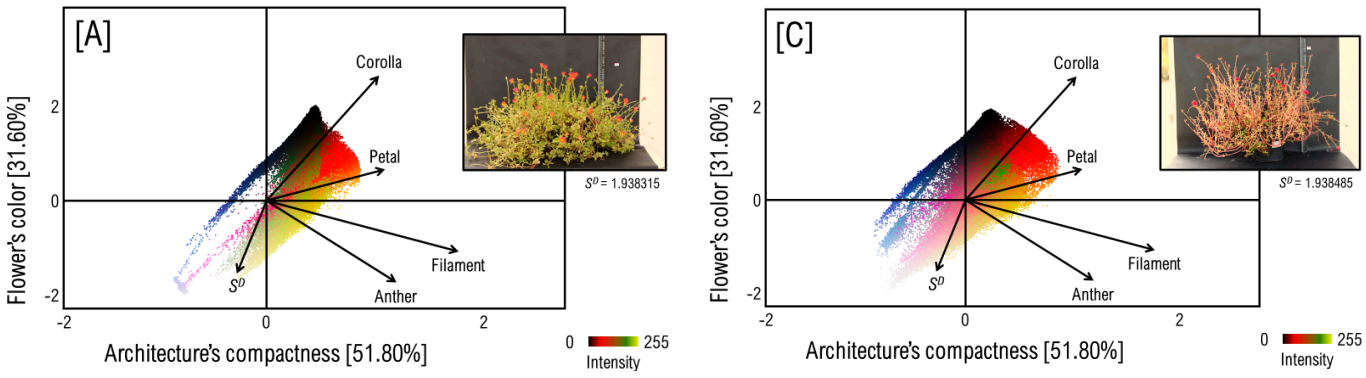

Figure 5. *Cont.*

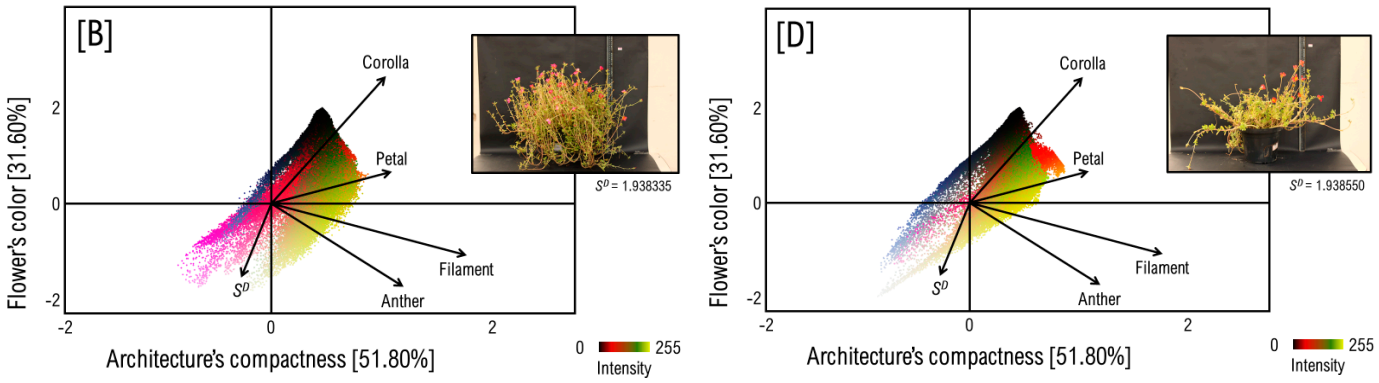

Figure 5. Mapping the botanical and computational features of flower and the architecture of red-flower samples of *P. umbraticola*. The sequence of alphanumerical symbols, from (**A**–**D**), relates to the increasing fractality of the pattern in the representation of the digital image.

The PCA allowed for the establishment of functional relationships between features of botany and image for white-flower samples, where the stems visually were not uncommonly greenish (Figure 2A). However, it did not work properly in discretizing imagery data on yellow-flower (Figure 2B) and red-flower (Figure 2C) samples. The stems of yellow-flower and red-flower individuals of *P. umbraticola* were glossy and purplish, making them "confounding" eigenvectors for the biophysical modeling. A graphical characteristic of such confounders in the process of orthogonalization referred to a larger proportion of low-intensity pixels in the right upper quadrant of all sublevel bi-plot diagrams on yellow-flower (Figure 4) and red-flower (Figure 5) samples, even though yellow-flower samples were visually distinctive in the proportion of leaves and stem in the image, and realistically they were graphically similar. Therefore, purplish stems introduced non-random variability into the dataset, "confounding" the algorithm in photogrammetrically reconstructing the spectral signatures of yellow-flower samples. The misinformation-to-information overlap was clearer in red-flower samples (Figure 5). Other than the purplish stems, the bright yellowish pattern consisting of anthers and filaments in the central region of the reddish flower (Figure 2C) also created or masked the true pixel's intensity, making such parts potential sources of confounding; hence, mapping the inputs to the output became rather complex. Once we have visualized through PCA the negative impact of confounders on the quality of the raw dataset, we decided to segment the representation of an image into something more meaningful and easier to analyze than the parent photo, namely a super-pixel. Thereby, we fitted a sigmoid Gompertz function to data with and without pixel-wise over-segmentation through the SLIC algorithm to illustrate and convey the importance of isolating the confounder from the dataset to address biophysical modeling with greater accuracy.

3.3. Predicting in the Gompertz Model for the Superpixel-Wise Intensity of Flower's Color upon the Fractal Dimension of Architecture

The SLIC algorithm segmented the high-resolution photos (Figure 6A) into a set of compact and uniform superpixels (Figure 6D). The cutting-edge image-processing solution grouped the pixels by chromatic similarity and topological proximity merely as a result of processing low-intensity features, without computational unfeasibility. Thus, it assisted the sigmoid Gompertz function in statistically describing the functional relationship between the intensity of the flower's color and the fractal dimension of the plant's architecture with greater accuracy (r_{adj}^2~0.80) than what would be possible in dealing with data without segmentation (Figure 7).

Figure 6. Major steps of the processing of the image in predicting the pixel-wise intensity of the flower's color upon the fractality of architecture of *P. umbraticola*; labeling (**A**), equalization (**B**), quantization (**C**), segmentation (**D**), and binarization (**E**).

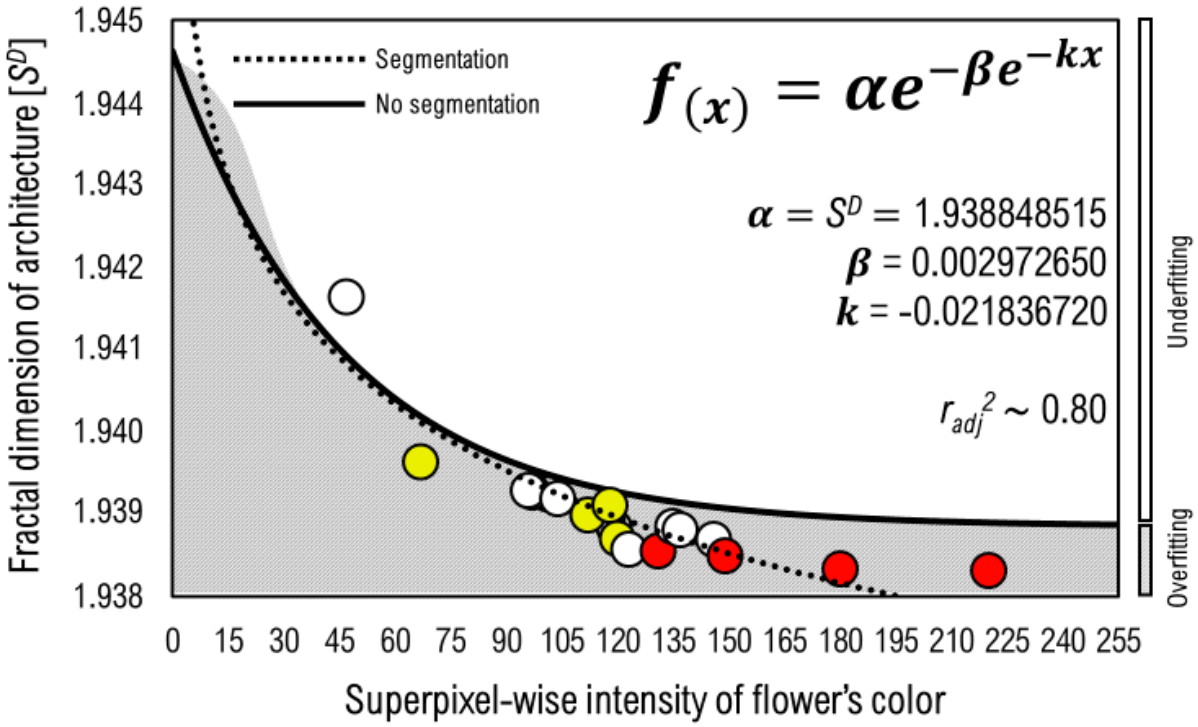

Figure 7. Predicting via Gompertz function the pixel-wise intensity of flower's color upon the fractal dimension of architecture from high-resolution imagery data on white-color, yellow-color, and red-color varieties of *P. umbraticola*.

By analyzing the breakthrough curves (Figure 7), the relationship between fractal architecture's compactness and the intensity of the flower's color was positive. Therefore, the more compact or visually smoother the architecture (S^D closer to 1), the more intensive the color of the flowering structure. In contrast, an architecturally more complex or rougher (S^D closer to 2) canopy is not likely to produce vibrant flowers, and thus the intensity of pixel can decrease in the digital representation of an image. Comparatively, raw imagery data (solid line) were likely to introduce a larger proportion of systematic errors into the biophysical modeling than imagery data with superpixel segmentation (dotted line). Thereby, the Gompertz approach was likely to either underfit to data on white-flower samples or overfit to data on yellow-color and red-flower samples.

Scatter dots corresponding to white-flower samples closest to the solid line supported the biasing role of botanical confounders in biophysical modeling. In contrast, scatter dots graphically representing yellow-flower and red-flower samples farthest from the solid line supported the introduction of non-random variability in the process by botanical confounders. Furthermore, the dotted line closer to observations than the solid line supported the importance of superpixel segmentation to bring more accurate and reliable predictive data analytics into implementation. Generally, the sigmoid Gompertz function proved to be useful in predicting the superpixel-wise intensity of the flower's color upon the architectural fractality, and the application of the SLIC algorithm notably updated both parametrization and adequacy of the biophysical model (Table 1).

Table 1. Parametrization and adequacy of predicting in the sigmoid Gompertz function for the superpixel-intensity of flower's color upon the architecture's fractality.

Parameter	No Segmentation	Segmentation
α	1.923799685 *	1.937848515 **
β	0.002972565 *	0.002972670 *
k	−0.220573050 **	−0.228367205 **
r_{adj}^2	0.725	0.80

Significant code: ** p-value < 0.01; * p-value < 0.05.

4. Discussion

4.1. Insights into Biophysical Modeling

Even though *P. umbraticola* was architecturally complex, the SLIC algorithm and BCM proved to be a breakthrough merger for extracting useful imagery data to predict the intensity of a flower's color upon the fractal dimension of a plant's architecture and describe how the variety of inflorescence can impact the biophysical modeling. By analyzing the *P. umbraticola* botanically, we see that it is a not uncommonly fleshy graceful herb. Every leaf is visually simple, alternate or opposite, subsessile, and exstipulate. Every inflorescence is an axillary cyme or panicle, comprising actinomorphic and often showy (vibrant) flowers (Figure 1). The calyx consists of twin sepals and the corolla consists of 4–6 ephemeral petals. The stems are smooth, glossy, and purplish, making them a source of confounding features in the processing of creating the digital image.

"Confounder" is any variable capable of creating or masking interactions with an outcome [38]. Because it can induce a dependency structure between input and output, diagnosing it from the original dataset is not easy. Even though an artefactual variable does not typically impact the performance of an algorithm, ignoring it can produce an unrealistic outcome. Furthermore, the model cannot perform as we might expect on data without a confounding input–output relationship. The PCA in this study can capture the confounding role of purplish stems in the photogrammetric reconstruction of red-flower samples (Figure 5D). The introduction of non-random variability into the biophysical modeling by confounders can make it challenging for the algorithm to calculate true relationships between the vectorial inputs, namely corolla, petal, filament, and anther, and the pixel's intensity as the output.

Even though PCA was capable of summarizing the structure of high-dimensional data into latent hits, it was not sufficient to effectively discretize the confounding effect of purplish stems on the quality of imagery data on red-flower samples. Thus, the data-reduction multivariate technique did relate imprecisely low-intensity pixels to high-intensity pixels corresponding to vibrant inflorescences in the multifactorial biophysical model, making it challenging to attribute the dependence of the intensity of the flower's color on the canopy's architecture. This subtle pitfall becomes harder to handle on architecturally more complex samples, where absent vegetative structures further contributed to the proportion of low-intensity pixels, creating unrealistic interactions, or rather masking true relationships between botanical and computational features.

By segmenting the representation of an image into a set of superpixels, we can analyze particular objects and boundaries with greater accuracy than would be possible in dealing with raw data (without segmentation). A set of pixels in a region of the image is similar regarding topological proximity and color intensity, making it distinctive from another adjacent set. The powerfulness of the SLIC algorithm towards segmenting the image into k-connection superpixels can isolate the confounding effect of the bright yellow region in the red flower. Hence, it can enable the Gompertz function to more accurately predict the color's intensity upon the canopy's architecture. However, it is not likely to be effective in improving the quality of imagery data on white-flower and yellow-flower samples since the colors of the anther and the whole reproductive organ are the same. Such botanical features can make it easier for the data-rotating algorithm to discretize high-intensity pixels towards flowers in parts of the plant where the distribution of stems and leaves is nearly uniform.

4.2. The Value of This Study to Develop High-Throughput Phenotyping and the Ways Forward

While we cannot still prove whether our imagery protocol is feasible at an industrial scale, our experimental study can provide further knowledge to progress the field's prominence in developing high-throughput phenotyping technologies. Even though values of S^D tightly ranged from 1.938315 to 1.941630, the box-counting algorithm proved to be useful in extracting an indicator for the "architectural complexity" of the object from its high-resolution digital representation, straightforwardly, accurately and objectively, which would not be possible with traditional analytical approaches. Most importantly, it allowed for predicting using sigmoid Gompertz function for the intensity of a flower's color upon the fractal dimension of the architecture with great accuracy, even greater by processing superpixel-wise data. As S^D came closer to 2, the BCM validated the irregular architecture of *P. umbraticola*, which is challenging and would not be possible to assess by applying Euclidian theory geometry. Such a mathematical approach does apply strictly to regular patterns and so would not measure the dimension of a plant's architecture as BCM did precisely, without any computational unfeasibility. Therefore, BCM was key to bringing our breakthrough imagery protocol to implementation in a successful way. An explanatory relationship between the superpixel-wise intensity of flower's color and fractal dimension of plant's architecture will likely enable stakeholders (e.g., breeders) not to spend resources investigating meaningless and subjective features, so they would better understand both process and product in order to reach a higher level of performance and ensure the reliable application of the technology. As plant breeding programs become more data-driven, our framework would make it better for evolving these without obscuring insightful relationships, or rather with greater objectiveness and accuracy than would be possible with traditional phenotyping interventions.

This study is an important part of transdisciplinary research, elaborating conceptual, theoretical, methodological, and translational innovations toward high-throughput phenotyping. Our imagery protocol is still at an early stage of research and development. However, it proved to be useful in establishing a functional relationship between the superpixel-wise intensity of the flower's color and the fractal dimension of the architecture of *P. umbraticola*, which we grew in a protected environment to isolate the negative impact of any stressing agent on the quality of image data and predictive performance

of the framework. We set out the *P. umbraticola* as a model for ornamentals, because of its characteristic showy inflorescence and irregular external shape. These outstanding features opened the possibility of developing an accurate and reliable biophysical model, supporting the hypothesis of this study. Therefore, further in-depth investigations that integrate and move beyond discipline-specific approaches will concentrate on analyzing field-level imagery data on oilseed crops (e.g., soybean and sunflower) to cross-validate and position our innovative solution for high-throughput phenotyping in the real world. We will pay an adequate emphasis to the environment and how it can interact with the subject of analysis to determine morphophysiological features, in order to improve the soundness of our breakthrough strategy for improving the control of the visual quality and breeding of economically valuable crops.

5. Conclusions

This explanatory study demonstrated the possibility of predicting the intensity of the flower's color upon the fractal dimension of architecture from high-resolution imagery data on *P. umbraticola*. The more compact the herbaceous structure of the crop, the more intensive the color of the flower. The fractal dimension of architecture and intensity of the flower's color are reliable descriptors for the botanical–computational nexus, making them drivers to bring accurate biophysical models into implementation. Morphophysiological features, such as purplish glossy stems in yellow-flower individuals and bright yellowish anthers in red-flower individuals, can act as confounders for the processing of images and modeling. However, the SLIC algorithm can isolate them from the dataset, making it possible for mapping the superpixel-wise intensity of a flower's color to the fractal dimension of architecture with greater accuracy. Therefore, insights into the conceptual and technical ramifications of this paper will likely provide further knowledge to progress the field's prominence in developing high-throughput phenotyping, whether for improving the control of the visual quality or breeding of *P. umbraticola*.

Supplementary Materials: The following supporting information can be downloaded at: https://www.mdpi.com/article/10.3390/agronomy12061342/s1. Table S1: Principal components analysis for the pixel-wise intensity-fractality nexus in processing imagery data on *P. umbraticola*.

Author Contributions: Conceptualization, J.d.S.S. and B.R.d.A.M.; Data curation, J.d.S.S. and B.R.d.A.M.; Formal analysis, L.M.P.; Investigation, J.d.S.S., L.M.P. and B.R.d.A.M.; Methodology, J.d.S.S. and B.R.d.A.M.; Project administration, J.d.S.S. and E.R.d.R.; Resources, E.R.d.R.; Supervision, S.H.U.-T.; Validation, J.d.S.S., L.M.P. and B.R.d.A.M.; Visualization, J.d.S.S., L.M.P., B.R.d.A.M., E.R.d.R. and S.H.U.-T.; Writing—original draft, J.d.S.S., L.M.P. and B.R.d.A.M.; Writing—review & editing, J.d.S.S., L.M.P. and B.R.d.A.M. All authors have read and agreed to the published version of the manuscript.

Funding: This is work was supported by the Coordination for the Improvement of Higher Education Personnel (CAPES, scholarship code No. 001), National Council for Scientific and Technological Development (CNPq, award No. 442104/2019-7), and the Pró-reitoria de Pós-Graduação (PROPG).

Informed Consent Statement: Not applicable.

Data Availability Statement: Not applicable.

Acknowledgments: We would like to acknowledge the funding sponsors of this work and also the Plant Biotechnology Laboratory of the Federal University of Paraiba for the infrastructural support.

Conflicts of Interest: The authors declare no conflict of interest.

References

1. Giraldo, J.P.; Wu, H.; Newkirk, G.M.; Kruss, S. Nanobiotechnology Approaches for Engineering Smart Plant Sensors. *Nat. Nanotechnol.* **2019**, *14*, 541–553. [CrossRef] [PubMed]
2. Lowry, G.V.; Avellan, A.; Gilbertson, L.M. Opportunities and Challenges for Nanotechnology in the Agri-Tech Revolution. *Nat. Nanotechnol.* **2019**, *14*, 517–522. [CrossRef] [PubMed]

3. Afshin, A.; Sur, P.J.; Fay, K.A.; Cornaby, L.; Ferrara, G.; Salama, J.S.; Mullany, E.C.; Abate, K.H.; Abbafati, C.; Abebe, Z.; et al. Health Effects of Dietary Risks in 195 Countries, 1990–2017: A Systematic Analysis for the Global Burden of Disease Study 2017. *Lancet* **2019**, *393*, 1958–1972. [CrossRef]
4. Nordhagen, S.; Lambertini, E.; DeWaal, C.S.; McClafferty, B.; Neufeld, L.M. Integrating Nutrition and Food Safety in Food Systems Policy and Programming. *Glob. Food Secur.* **2022**, *32*, 100593. [CrossRef]
5. Shahzad, A.N.; Qureshi, M.K.; Wakeel, A.; Misselbrook, T. Crop Production in Pakistan and Low Nitrogen Use Efficiencies. *Nat. Sustain.* **2019**, *2*, 1106–1114. [CrossRef]
6. Spanaki, K.; Karafili, E.; Sivarajah, U.; Despoudi, S.; Irani, Z. Artificial Intelligence and Food Security: Swarm Intelligence of AgriTech Drones for Smart AgriFood Operations. *Prod. Plan. Control.* **2021**, *18*, 1–19. [CrossRef]
7. Zhang, R.; Wu, J.; Zhao, Y.; He, X.; Wang, R. Numerical Simulation of the Feasibility of Supercritical CO_2 Storage and Enhanced Shale Gas Recovery Considering Complex Fracture Networks. *J. Pet. Sci. Eng.* **2021**, *204*, 108671. [CrossRef]
8. Deléglise, H.; Interdonato, R.; Bégué, A.; Maître d'Hôtel, E.; Teisseire, M.; Roche, M. Food Security Prediction from Heterogeneous Data Combining Machine and Deep Learning Methods. *Expert Syst. Appl.* **2022**, *190*, 116189. [CrossRef]
9. Valoppi, F.; Agustin, M.; Abik, F.; Morais de Carvalho, D.; Sithole, J.; Bhattarai, M.; Varis, J.J.; Arzami, A.N.A.B.; Pulkkinen, E.; Mikkonen, K.S. Insight on Current Advances in Food Science and Technology for Feeding the World Population. *Front. Sustain. Food Syst.* **2021**, *5*, 385. [CrossRef]
10. Vinuesa, R.; Azizpour, H.; Leite, I.; Balaam, M.; Dignum, V.; Domisch, S.; Felländer, A.; Langhans, S.D.; Tegmark, M.; Fuso Nerini, F. The Role of Artificial Intelligence in Achieving the Sustainable Development Goals. *Nat. Commun.* **2020**, *11*, 233. [CrossRef]
11. Gardiner, L.-J.; Krishna, R. Bluster or Lustre: Can AI Improve Crops and Plant Health? *Plants* **2021**, *10*, 2707. [CrossRef] [PubMed]
12. Fahlgren, N.; Gehan, M.A.; Baxter, I. Lights, Camera, Action: High-Throughput Plant Phenotyping Is Ready for a Close-Up. *Curr. Opin. Plant. Biol.* **2015**, *24*, 93–99. [CrossRef] [PubMed]
13. Chacón, B.; Ballester, R.; Birlanga, V.; Rolland-Lagan, A.-G.; Pérez-Pérez, J.M. A Quantitative Framework for Flower Phenotyping in Cultivated Carnation (*Dianthus caryophyllus* L.). *PLoS ONE* **2013**, *8*, e82165. [CrossRef] [PubMed]
14. Xiong, J.; Yu, D.; Liu, S.; Shu, L.; Wang, X.; Liu, Z. A Review of Plant Phenotypic Image Recognition Technology Based on Deep Learning. *Electronics* **2021**, *10*, 81. [CrossRef]
15. Danin, A.; Buldrini, F.; Bandini Mazzanti, M.; Bosi, G.; Caria, M.C.; Dandria, D.; Lanfranco, E.; Mifsud, S.; Bagella, S. Diversification of *Portulaca oleracea* L. Complex in the Italian Peninsula and Adjacent Islands. *Bot. Lett.* **2016**, *163*, 261–272. [CrossRef]
16. Nybom, H.; Lācis, G. Recent Large-Scale Genotyping and Phenotyping of Plant Genetic Resources of Vegetatively Propagated Crops. *Plants* **2021**, *10*, 415. [CrossRef]
17. Chéné, Y.; Rousseau, D.; Lucidarme, P.; Bertheloot, J.; Caffier, V.; Morel, P.; Belin, É.; Chapeau-Blondeau, F. On the Use of Depth Camera for 3D Phenotyping of Entire Plants. *Comput. Electron. Agric.* **2012**, *82*, 122–127. [CrossRef]
18. Tu, S.; Xue, Y.; Zheng, C.; Qi, Y.; Wan, H.; Mao, L. Detection of Passion Fruits and Maturity Classification Using Red-Green-Blue Depth Images. *Biosyst. Eng.* **2018**, *175*, 156–167. [CrossRef]
19. Zhu, H.; Chu, B.; Fan, Y.; Tao, X.; Yin, W.; He, Y. Hyperspectral Imaging for Predicting the Internal Quality of Kiwifruits Based on Variable Selection Algorithms and Chemometric Models. *Sci. Rep.* **2017**, *7*, 7845. [CrossRef]
20. Boumaza, R.; Huché-Thélier, L.; Demotes-Mainard, S.; Coz, E.L.; Leduc, N.; Pelleschi-Travier, S.; Qannari, E.M.; Sakr, S.; Santagostini, P.; Symoneaux, R.; et al. Sensory Profiles and Preference Analysis in Ornamental Horticulture: The Case of the Rosebush. *Food Qual. Prefer.* **2010**, *21*, 987–997. [CrossRef]
21. Evers, J.B.; van der Krol, A.R.; Vos, J.; Struik, P.C. Understanding Shoot Branching by Modelling Form and Function. *Trends Plant Sci.* **2011**, *16*, 464–467. [CrossRef] [PubMed]
22. Dornbusch, T.; Wernecke, P.; Diepenbrock, W. Description and Visualization of Graminaceous Plants with an Organ-Based 3D Architectural Model, Exemplified for Spring Barley (*Hordeum vulgare* L.). *Vis. Comput.* **2007**, *23*, 569–581. [CrossRef]
23. Vos, J.; Evers, J.B.; Buck-Sorlin, G.H.; Andrieu, B.; Chelle, M.; de Visser, P.H.B. Functional–Structural Plant Modelling: A New Versatile Tool in Crop Science. *J. Exp. Bot.* **2010**, *61*, 2101–2115. [CrossRef]
24. Bertheloot, J.; Wu, Q.; Cournède, P.-H.; Andrieu, B. NEMA, a Functional–Structural Model of Nitrogen Economy within Wheat Culms after Flowering. II. Evaluation and Sensitivity Analysis. *Ann. Bot.* **2011**, *108*, 1097–1109. [CrossRef] [PubMed]
25. de Jesus, O.N.; Lima, L.K.S.; Soares, T.L.; da Silva, L.N.; dos Santos, I.S.; Sampaio, S.R.; de Oliveira, E.J. Phenotypic Diversity and Alternative Methods for Characterization and Prediction of Pulp Yield in Passion Fruit (*Passiflora* Spp.) Germplasm. *Sci. Hortic.* **2022**, *292*, 110573. [CrossRef]
26. Zhang, C.; Serra, S.; Quirós-Vargas, J.; Sangjan, W.; Musacchi, S.; Sankaran, S. Non-Invasive Sensing Techniques to Phenotype Multiple Apple Tree Architectures. *Inf. Processing Agric.* **2021**. [CrossRef]
27. Hu, Y.; Shen, J.; Qi, Y. Estimation of Rice Biomass at Different Growth Stages by Using Fractal Dimension in Image Processing. *Appl. Sci.* **2021**, *11*, 7151. [CrossRef]
28. Ramos, G.Q.; Matos, R.S.; Filho, H.D.d.F. Advanced Microtexture Study of *Anacardium occidentale* L. Leaf Surface From the Amazon by Fractal Theory. *Microsc. Microanal.* **2020**, *26*, 989–996. [CrossRef]
29. Dhal, K.G.; Das, A.; Ray, S.; Gálvez, J.; Das, S. Histogram Equalization Variants as Optimization Problems: A Review. *Arch. Comput. Methods Eng.* **2021**, *28*, 1471–1496. [CrossRef]
30. Pérez-Delgado, M.-L. Color Image Quantization Using the Shuffled-Frog Leaping Algorithm. *Eng. Appl. Artif. Intell.* **2019**, *79*, 142–158. [CrossRef]

31. He, F.; Parvez Mahmud, M.A.; Kouzani, A.Z.; Anwar, A.; Jiang, F.; Ling, S.H. An Improved SLIC Algorithm for Segmentation of Microscopic Cell Images. *Biomed. Signal. Processing Control* **2022**, *73*, 103464. [CrossRef]
32. Khairnar, S.; Thepade, S.D.; Gite, S. Effect of Image Binarization Thresholds on Breast Cancer Identification in Mammography Images Using OTSU, Niblack, Burnsen, Thepade's SBTC. *Intell. Syst. Appl.* **2021**, *10–11*, 200046. [CrossRef]
33. Panigrahy, C.; Seal, A.; Mahato, N.K.; Bhattacharjee, D. Differential Box Counting Methods for Estimating Fractal Dimension of Gray-Scale Images: A Survey. *Chaos Solitons Fractals* **2019**, *126*, 178–202. [CrossRef]
34. Russ, J.C. *The Image Processing Handbook*, 5th ed.; CRC Press: Boca Raton, FL, USA, 2006; ISBN 978-0-429-20692-4.
35. Zheng, C.; Sun, D.-W. 2—Image Segmentation Techniques. In *Computer Vision Technology for Food Quality Evaluation*; Sun, D.-W., Ed.; Food Science and Technology; Academic Press: Amsterdam, The Netherlands, 2008; pp. 37–56. ISBN 978-0-12-373642-0.
36. R: The R Project for Statistical Computing. Available online: https://www.r-project.org/ (accessed on 27 April 2020).
37. Tjørve, K.M.C.; Tjørve, E. The Use of Gompertz Models in Growth Analyses, and New Gompertz-Model Approach: An Addition to the Unified-Richards Family. *PLoS ONE* **2017**, *12*, e0178691. [CrossRef] [PubMed]
38. LeCun, Y.; Bengio, Y.; Hinton, G. Deep Learning. *Nature* **2015**, *521*, 436–444. [CrossRef]